Periodic vortex structures in superfluid ^{3}He-*A*

J. M. Karimäki* and E. V. Thuneberg
Low Temperature Laboratory, Helsinki University of Technology, 02150 Espoo, Finland
(Received 16 February 1999)

We discuss the general properties of periodic vortex arrangements in rotating superfluids. The different possible structures are classified according to the symmetry space groups and the circulation number. We calculate numerically several types of vortex structures in superfluid ^{3}He-*A*. The calculations are done in the Ginzburg-Landau region, but the method is applicable at all temperatures. A phase diagram of vortices is constructed in the plane formed by the magnetic field and the rotation velocity. The characteristics of the six equilibrium vortex solutions are discussed. The vortex sheet forms the equilibrium state of rotating ^{3}He-*A* at rotation velocities exceeding 2.6 rad/s. The results are in qualitative agreement with experiments. [S0163-1829(99)00741-9]

A superfluid cannot rotate homogeneously. Instead, quantized vortex lines are present in the equilibrium rotating state of superfluid ^{4}He. In superfluid ^{3}He the rotating states are more diverse. It has been discussed recently by Parts *et al.*[1] that four different types of vortices have been found experimentally in the superfluid *A* phase of ^{3}He. In this paper we present theoretical studies concerning the vortices observed in ^{3}He-*A*.

Some of the theoretical results that we presented in Refs. 1 and 2 were found to be incorrect in further calculations. These errors are corrected here. As a consequence, the present phase diagram of vortices differs from the one in Refs. 1 and 2. In particular, there appears a different vortex structure, the locked vortex 3, but also the locations of other phase boundaries are changed.

For introduction to superfluid ^{3}He (Refs. 3 and 4) and its vortices[5–9,2] we refer to various review articles. Although not introductory, this paper intends to be a complete exposition of what is needed for understanding the equilibrium vortex structures in bulk superfluid ^{3}He-*A*.

We start in Sec. I with the formulation of the vortex problem, which is general enough for all superfluids and can be generalized also to superconductors. This gives a general classification of vortex states based on space-group symmetry and circulation number. The classification is continued in Sec. II using properties specific to ^{3}He-*A*. The calculations of the vortex structures are based on the hydrostatic theory, which is discussed in Sec. III, and the calculational method is described in Sec. IV. Detailed description of the different vortex types is given in Sec. V. The correspondence with experiments is discussed in Sec. VI.

I. GENERAL VORTEX PROBLEM

Let us consider an uncharged fluid (in practice liquid ^{4}He, ^{3}He, or a quantum gas) in a container rotating at angular velocity $\mathbf{\Omega}$. We will neglect all complications arising from the finite size of the container. Although we will not discuss the detailed correspondence, the analysis in this section is also applicable to a charged fluid (superconductor) when $\mathbf{\Omega}$ is replaced by the averaged magnetic field $\mathbf{B}$.

At the microscopic level, the fluid has the effective Hamiltonian $H_{\rm eff}=H_0-\mathbf{\Omega}\cdot\mathbf{J}$. Here $H_0=\Sigma_i(p_i^2/2m)+V$ is the Hamiltonian in a nonrotating system, which consists of a kinetic energy term and an interaction energy term V. The angular momentum $\mathbf{J}=\Sigma_i[\frac{1}{2}(\mathbf{r}_i\times\mathbf{p}_i-\mathbf{p}_i\times\mathbf{r}_i)+\mathbf{S}_i]$ consists of an orbital and a spin part. We can write $H_{\rm eff}$ in the form

$$H_{\rm eff}=\sum_i \frac{1}{2m}(\mathbf{p}_i-m\mathbf{v}_{{\rm n},i})^2+V-\sum_i \mathbf{\Omega}\cdot\mathbf{S}_i-\sum_i \frac{1}{2}mv_{{\rm n},i}^2, \tag{1}$$

where $\mathbf{v}_{{\rm n},i}=\mathbf{\Omega}\times\mathbf{r}_i$ is the ''normal fluid'' velocity at the location of the particle i. The last term is the centrifugal energy. It causes the pressure to increase with increasing distance from the rotation axis. In principle, this term prohibits a strictly periodic vortex arrangement. However, it is very small at experimentally relevant rotation velocities and container sizes, so that we can safely neglect it. We will neglect also the second-last term because it vanishes in ^{4}He ($S=0$), and is very small in ^{3}He, where it corresponds to a magnetic field of $\approx 0.1\,\mu$T at a typical $\Omega=1$ rad/s. Because the rest of the paper is based on the reduced $H_{\rm eff}$, we write it again:

$$H_{\rm eff}=\sum_i \frac{1}{2m}(\mathbf{p}_i-m\mathbf{v}_{{\rm n},i})^2+V. \tag{2}$$

We will classify the rotating states according to their symmetries. For that purpose we first list all the symmetries of the Hamiltonian (2). They are (i) arbitrary translations, (ii) arbitrary rotations around $\mathbf{\Omega}$ (∞_z), (iii) the combination ($2'_x$) of time inversion ($'$) and rotation by the angle π (2) around an axis perpendicular to $\mathbf{\Omega}$, (iv) the reflection (m_z) in the plane perpendicular to $\mathbf{\Omega}$, (v) the combination (m'_x) of time inversion and reflection in a plane containing $\mathbf{\Omega}$, and (vi) all combinations of these operations. For each operation we have indicated a symbol in parentheses. They follow the international notation of crystallography[10] with a prime added

 ©1999 The American Physical Society

to denote time inversion.[11] Throughout this paper we use a rectangular coordinate system xyz where the z axis is parallel to $\mathbf{\Omega}$.

It is not completely obvious that the translations perpendicular to $\mathbf{\Omega}$ are symmetry operations of $H_{\rm eff}$ (2). This problem is equivalent to the case of electrons in uniform magnetic field,[12] and the corresponding problem for superfluid order parameter is discussed below. Another noteworthy feature is that both m_x and 2_x appear in combination with the time inversion. Otherwise these operations would not preserve the direction of the axial vector $\mathbf{\Omega}$.

Generally, the physical system either has all the symmetries of the Hamiltonian, or alternatively, one or more of the symmetries are broken. An ordinary fluid would preserve all the symmetries of the rotating Hamiltonian (2). This is not the case for a superfluid. We will show below that at least part of the translation symmetry is broken in the superfluid state when $\Omega \neq 0$.

The fundamental property of superfluidity is that one quantum state becomes macroscopically occupied. This condensate is described by an order parameter $A(\mathbf{r})$. The order parameter can be a scalar, as in ^{4}He, or a more complicated object. We associate a velocity field $\mathbf{v}_{\rm s}$ to the particles in the condensate. There is no general expression for the superfluid velocity $\mathbf{v}_{\rm s}$ in terms of $A(\mathbf{r})$. Also, several different velocities $\mathbf{v}_{\rm s}$ can exist, for example, one for spin-up and another for spin-down particles. Irrespective of the precise definition, we only need to know how $\mathbf{v}_{\rm s}$ changes in a gauge transformation. We require that the velocity associated with the order parameter $\exp[{\rm i}\phi(\mathbf{r})]A^{(0)}(\mathbf{r})$ is $\mathbf{v}_{\rm s}=(\hbar/M)\boldsymbol{\nabla}\phi(\mathbf{r})+\mathbf{v}_{\rm s}^{(0)}$, where $\mathbf{v}_{\rm s}^{(0)}$ is the velocity corresponding to $A^{(0)}(\mathbf{r})$. Here M is a mass that depends on the particular system. It equals the atomic mass for ^{4}He ($M=m_4$) and twice the atomic mass for ^{3}He ($M=2m_3$).

It is now obvious that $A(\mathbf{r})$ cannot be constant and also a phase factor $\exp[{\rm i}\phi(\mathbf{r})]$ times a constant is not allowed. The reason is that the kinetic energy term in the Hamiltonian (2) would grow faster than linearly with the volume of the system because $\mathbf{v}_{\rm s}$ would be constrained by $\oint \mathbf{v}_{\rm s}\cdot d\mathbf{r}=0$ and could not imitate $\mathbf{v}_{\rm n}=\mathbf{\Omega}\times\mathbf{r}$ on a large scale.

Our basic assumption is that the equilibrium structure of the rotating superfluid is periodic in space. It follows from above that the minimum period has to be finite at least in one direction, which is not parallel to $\mathbf{\Omega}$. We do not make here any assumption whether the translation symmetry is discrete or continuous in the two other linearly independent directions.

Crystalline materials are classified according to their symmetry into 1651 magnetic space groups. The most effective way to label these is the international crystallographic notation.[10,11] We use the same notation to label the space groups of rotating superfluids. This is possible because corresponding to every rotating state there exists at least one space group of a crystal. The reasons for this are that (i) the symmetries of the rotating-fluid problem listed above are a subgroup of those possible for a crystal, and (ii) no new symmetry groups appear even if one or two of the translation symmetries in a rotating superfluid were continuous.

Not all the 1651 magnetic space groups are relevant for rotating fluids. First, the time inversion is present in a rotating superfluid in a trivial way. In the generating symmetry operations it appears in combinations with m_x and 2_x, and only with them. Thus, by simply ignoring the time inversion, one can construct a one-to-one mapping from symmetry operations of a rotating fluid into symmetry operations that do not contain the time inversion.[13] Thus it is sufficient to limit to the 230 crystallographic space groups, which do not include the time-inversion operation. Second, the number of relevant groups is further reduced because a rotation axis higher than 2 is allowed in the direction of $\mathbf{\Omega}$ only. This implies that cubic groups are not acceptable. The remaining 194 space groups each give rise to 1, 2, or 3 different symmetry groups of rotating fluids. This is because some of the crystal groups can be oriented in different ways relative to the $\mathbf{\Omega}$ direction.

What has been said above about symmetry does not directly apply to the order parameter $A(\mathbf{r})$. The reason is that this complex quantity has phase ϕ, which is not an observable quantity. Therefore, instead of being strictly periodic, $A(\mathbf{r})$ is only quasiperiodic:

$$A(\mathbf{r}+\mathbf{a}_k)=\exp[{\rm i}\phi_k(\mathbf{r})]A(\mathbf{r}). \tag{3}$$

Here $\mathbf{a}_k$ are three linearly independent translation vectors ($k=1$, 2, and 3) and $\phi_k(\mathbf{r})$ are the corresponding phase shifts. Similar phase factors occur also in rotations, reflections, and time inversions. The quantity that has to be periodic in lattice translations is $\mathbf{v}_{\rm s}-\mathbf{v}_{\rm n}$. This gives a constraint for the phase shifts $\phi_k(\mathbf{r})$. Using the gauge invariance for $\mathbf{v}_{\rm s}$, one finds $\boldsymbol{\nabla}\phi_k(\mathbf{r})=\tilde{\mathbf{\Omega}}\times\mathbf{a}_k$. In order to simplify the formulas, we will repeatedly use the notation $\tilde{\mathbf{\Omega}}=(M/\hbar)\mathbf{\Omega}$. The gradient of ϕ_k is trivially integrated to[14]

$$\phi_k(\mathbf{r})=C_k+\tilde{\mathbf{\Omega}}\times\mathbf{a}_k\cdot\mathbf{r}, \tag{4}$$

where C_k are constants of integration. An implicit requirement here is that $\mathbf{v}_{\rm s}$ is defined on the path of integration. We assume that the regions where $\mathbf{v}_{\rm s}$ is undefined are at most one-dimensional. In this case it seems possible to choose the unit cell of the translation lattice so that $\mathbf{v}_{\rm s}$ is well defined along all its edges.

An important requirement is that the lattice-translation rule (3) is consistent with a uniquely defined $A(\mathbf{r})$. We express $A(\mathbf{r}+\mathbf{a}_i+\mathbf{a}_j)$ as a function of $A(\mathbf{r})$ using the translation rule twice. The result should be independent of the order in which the two translations by $\mathbf{a}_i$ and $\mathbf{a}_j$ are done. This gives the condition

$$\tilde{\mathbf{\Omega}}\cdot\mathbf{a}_i\times\mathbf{a}_j=\pi\sum_k e_{ijk}N_k, \tag{5}$$

where N_k are integers and e_{ijk} the fully antisymmetric tensor.

The lattice translation vectors $\mathbf{a}_k$ can be chosen in several different ways. Next we want to redefine the set $\{\mathbf{a}_k\}$ so that it is optimal for further analysis. The new $\mathbf{a}_3$ can always be chosen parallel to $\mathbf{\Omega}$. Namely, setting $\mathbf{a}_3=\Sigma_k N_k\mathbf{a}_k^{\rm old}$, it follows from Eq. (5) that $\mathbf{a}_3\times\mathbf{\Omega}=0$. Applying Eq. (5) to a new linearly independent set $\{\mathbf{a}_k\}$, we find that $N_1=N_2=0$ but $N_3\neq 0$. The nonzero integer value of N_3 implies that a continuous translation symmetry can exist only in the direction of $\mathbf{\Omega}$. We can therefore additionally require that $\mathbf{a}_1$ and $\mathbf{a}_2$ are primitive translation vectors, i.e., they correspond to the minimum (positive) value of $\mathbf{\Omega}\cdot\mathbf{a}_1\times\mathbf{a}_2$.

We define the circulation number N as equal to N_3 (5) corresponding to primitive $\mathbf{a}_1$ and $\mathbf{a}_2$:

$$\tilde{\mathbf{\Omega}} \cdot \mathbf{a}_1 \times \mathbf{a}_2 = \pi N. \tag{6}$$

Similar to the symmetry groups, the different values of N can be used to classify the rotating states. N is called the circulation number because it is related to the circulation of the superfluid velocity around a primitive cell

$$N = \frac{1}{2\pi} \oint_{\text{primitive cell}} d\mathbf{r} \cdot \tilde{\mathbf{v}}_s, \tag{7}$$

where $\tilde{\mathbf{v}}_s = (M/\hbar)\mathbf{v}_s$. We note that the limitation to the boundary of the primitive cell in Eq. (7) is crucial in ^{3}He-A, where the circulation is not generally quantized.

Let us consider the case that there is a continuous translation symmetry along $\mathbf{\Omega}$. This is an important case because all known vortex types belong to this category. However, very few general properties can be listed in addition to those ones already mentioned above. The main simplification is that the primitive translation vectors $\mathbf{a}_1$ and $\mathbf{a}_2$ can be chosen perpendicular to $\mathbf{\Omega}$. These generate a two dimensional Bravais lattice. Thus these rotating states can be classified into five categories according to the symmetry of the two-dimensional (2D) lattice:[10] oblique, square, hexagonal, primitive rectangular, and centered rectangular. The number of possible space groups is considerably larger. In particular, the 17 two-dimensional space groups listed in Ref. 10 are not sufficient for rotating states because they lack the operation m_z.

We illustrate the classification of vortices with known example cases. For a scalar order parameter (^{4}He) the Bravais lattice is hexagonal and $N=1$.[15] It has the symmetry group $P(6/m)(2'/m')(2'/m')$, or shortly $P6/mm'm'm'$. Generally, the international symbols consist of a letter followed by three symbol sets.[10] The letter shows the basis of the lattice, for example, P denotes a primitive and C a centered unit cell. The following three symbol sets describe symmetries with respect to three different inequivalent axes, respectively. The first $6/m$ indicates that there is a sixfold rotation symmetry and a reflection symmetry m, both with respect to the same axis. Here the sixfold axis has to be parallel to $\mathbf{\Omega}$ and thus the reflection plane is perpendicular to $\mathbf{\Omega}$. The second set $2'/m'$ describes a $2'$ symmetry and an m' symmetry with respect to an axis perpendicular to $\mathbf{\Omega}$. Finally, the third set $2'/m'$ describes the same symmetries around the third inequivalent axis of the hexagonal lattice.

The relative orientation of the space group and $\mathbf{\Omega}$ is usually revealed by the primes because the primed axes are always perpendicular to $\mathbf{\Omega}$. For some structures ($C12'1$, for example) pure symmetry considerations are insufficient to fix the direction of $\mathbf{\Omega}$. However, as proved below Eq. (5), the $\mathbf{\Omega}$ axis always coincides with one direction of translation symmetry. This is not a consequence of symmetry but arises from the divergent rigidity of the vortex lattice against tilt deformation at long wavelengths.[16]

As another example, we consider vortices of ^{3}He-B. Two types of fully stable vortices are known. An isolated A-phase core vortex has symmetry class $\infty m'$, and a double-core vortex $2m'm'$.[17] Here the symmetry breaking relative to $(\infty/m)(2'/m')$ arises from the core of each vortex. When these vortices form a lattice, the simplest possible structures have $N=1$, and the space groups are $P6m'm'$ and $Cm'm'2$, respectively. The lattice breaks the rotating symmetry of the A-phase-core vortex to sixfold, and the twofold rotation symmetry of the double-core vortex breaks the hexagonal lattice symmetry to centered rectangular. Both these effects are in practice very weak because the core sizes of the vortices in ^{3}He-B are much smaller than the distance between vortices.

The symmetry classification of vortices has previously been made only for point groups. This means that all the translations in the space group are ignored. Although this does not describe the whole lattice symmetry, there are several physical properties for which the point group gives a sufficient description.[6,18] We also comment on the notation. The symmetries $\overline{1}$, m'_y, $2'_y$ often appear in dealing with vortices of ^{3}He. Here $\overline{1}$ is the inversion and the subindexes in m'_y and $2'_y$ denote that they refer to the same axis. These operations give rise to five symmetry classes 1, $\overline{1}$, m', $2'$, and $2'/m'$. Here the first one contains only the unit element, the three middle ones have each one symmetry operation $\overline{1}$, m'_y, or $2'_y$, respectively, and the last one has all the three (because two of them imply the third). In Ref. 6, the same groups were labeled by letters o, u, v, w, and uvw, respectively. Still another notation is due to Schönflies, and this was used to denote the same classes in Ref. 18. Contrary to the international crystallographic symbols, these other notations do not allow a meaningful generalization to space groups.

Let us study the meaning of the constants C_k in Eq. (4). We will show that C_1 and C_2 can be put to zero without losing generality. We consider an arbitrary order parameter field $A^{(0)}(\mathbf{r})$. We construct from it another field $A(\mathbf{r})$ by doing a translation by an arbitrary vector $\mathbf{b}$ as follows:

$$A(\mathbf{r}) = \exp(i\tilde{\mathbf{\Omega}} \times \mathbf{b} \cdot \mathbf{r}) A^{(0)}(\mathbf{r} - \mathbf{b}). \tag{8}$$

This field obviously has the same energy as the original one because the phase factor takes care that the counterflow velocity $\mathbf{v} = \mathbf{v}_s - \mathbf{v}_n$ is unchanged: $\mathbf{v}(\mathbf{r}) = \mathbf{v}^{(0)}(\mathbf{r} - \mathbf{b})$. By straightforward calculation one can verify that the coefficients C_1 and C_2 for the new field are related to the old ones by $C_k = C_k^{(0)} + 2\tilde{\mathbf{\Omega}} \times \mathbf{b} \cdot \mathbf{a}_k$. Choosing $\mathbf{b}$ appropriately, one can put C_1 and C_2 to zero. Thus the significance of C_1 and C_2 is that their values fix the position of the vortex solution relative to the rotation center.

The coefficient C_3 in Eq. (4) is the phase shift in translations parallel to $\mathbf{\Omega}$. It is related to the superfluid velocity parallel to $\mathbf{\Omega}$. It often vanishes for symmetry reasons, but it can be nonzero for vortices of low symmetry. For example, consider a vortex with the symmetry group $C12'1$ and a continuous translation symmetry in the z direction. The only point symmetry operation $2'_x$ leaves the z component of the current unchanged. Thus such a vortex generally has a nonzero net superfluid current in the z direction even though $v_{s,z} = 0$. Depending on the boundary conditions at $z = \pm\infty$, this current may be compensated by a current arising from a nonzero $\tilde{v}_{s,z} = C_3/a_3$.

II. SUPERFLUID ^{3}He-A

The previous section showed that the vortex structures in any superfluid can be classified according to the circulation number and the space group. In this section we continue the classification using properties specific to ^{3}He-A.

The order parameter of bulk superfluid ^{3}He-A is a complex 3×3 matrix of the form[3,4]

$$\vec{A}=\Delta\hat{\mathbf{d}}(\hat{\mathbf{m}}+i\hat{\mathbf{n}}). \tag{9}$$

Here $\hat{\mathbf{d}}$, $\hat{\mathbf{m}}$, and $\hat{\mathbf{n}}$ are unit vectors and $\hat{\mathbf{m}}\perp\hat{\mathbf{n}}$. The amplitude Δ is a temperature- and pressure-dependent constant. It is conventional to define $\hat{\mathbf{l}}=\hat{\mathbf{m}}\times\hat{\mathbf{n}}$, so that $\hat{\mathbf{m}}$, $\hat{\mathbf{n}}$, and $\hat{\mathbf{l}}$ form an orthonormal set.

As a first step, the vortices are classified to ''continuous'' and ''singular.'' The former alternative means that the bulk form (9) with constant Δ forms a good approximation to the order parameter everywhere in the primitive cell. The latter alternative means that this is not the case. This classification may not be precise in general, but there is no difficulty for the six vortex types to be considered here: only the ''singular vortex'' is singular, the other four are continuous.

We note that only singular vortices exist for a scalar A because the amplitude of A has to vanish somewhere within the primitive cell of $N=1$. Continuous vortices are possible in ^{3}He-A because nonzero circulation can be generated by appropriate $\hat{\mathbf{m}}(\mathbf{r})$ and $\hat{\mathbf{n}}(\mathbf{r})$ fields.

The continuous structures can be further classified by the numbers

$$\nu_d=\frac{1}{4\pi}\int_{\text{primitive cell}}dx\,dy\,\hat{\mathbf{d}}\cdot\frac{\partial\hat{\mathbf{d}}}{\partial x}\times\frac{\partial\hat{\mathbf{d}}}{\partial y}, \tag{10}$$

$$\nu_l=\frac{1}{4\pi}\int_{\text{primitive cell}}dx\,dy\,\hat{\mathbf{l}}\cdot\frac{\partial\hat{\mathbf{l}}}{\partial x}\times\frac{\partial\hat{\mathbf{l}}}{\partial y}. \tag{11}$$

These numbers are integers because $\hat{\mathbf{d}}$ and $\hat{\mathbf{l}}$ are periodic. They describe how many times the mapping from the primitive cell to the vectors $\hat{\mathbf{d}}$ and $\hat{\mathbf{l}}$ covers the unit spheres.

The numbers N and ν_l are not independent. This follows from the definition of the superfluid velocity,

$$\tilde{\mathbf{v}}_s=\sum_i m_i\nabla n_i. \tag{12}$$

[As above, we use $\tilde{\mathbf{v}}=(2m_3/\hbar)\mathbf{v}$, where m_3 is the mass of a ^{3}He atom.] This implies the Mermin-Ho relation:[19]

$$\nabla\times\tilde{\mathbf{v}}_s=\frac{1}{2}\sum_{ijk}e_{ijk}l_i\nabla l_j\times\nabla l_k, \tag{13}$$

which together with Eqs. (7) and (11) gives

$$N=2\nu_l. \tag{14}$$

III. HYDROSTATIC THEORY

For a quantitative determination of the vortex structures we use an energy functional $F(A)$. In principle, it can be calculated from the effective Hamiltonian (2) as $F(A)=-T\ln[\mathrm{Tr}\exp(-H_{\text{eff}}/T)]$. This is a functional of $A(\mathbf{r})$ because the trace (Tr) is restricted to states having a given macroscopic $A(\mathbf{r})$. Various approximations for $F(A)$ are available: quasiclassical weak-coupling and weak-coupling-plus models, and phenomenological theories such as the Ginzburg-Landau theory and the hydrodynamic theory.

The basic assumption of the hydrodynamic theory is that the deviation of the order parameter $\vec{A}$ from the bulk form (9) is small. For this we have to require two conditions. (i) The magnetic field $\mathbf{H}$ should not be too large. In practice this condition excludes only a small region near the superfluid transition temperature T_c, where the A phase is distorted towards the A_1 phase.[4] (ii) The vectors $\hat{\mathbf{d}}(\mathbf{r})$, $\hat{\mathbf{m}}(\mathbf{r})$, and $\hat{\mathbf{n}}(\mathbf{r})$ are sufficiently slowly varying functions of the location $\mathbf{r}$. This implies that the hydrodynamic approach can be used for continuous vortices, but it is insufficient for singular ones.

Because of the slow variation, only terms up to the second order in the gradients of $\hat{\mathbf{d}}$, $\hat{\mathbf{m}}$, and $\hat{\mathbf{n}}$ are needed in the energy functional. The functional can be written as

$$F=\frac{1}{V}\int_V d^3r(f_d+f_h+f_g). \tag{15}$$

Here the volume V of integration is assumed to consist of an (arbitrary) integral number of unit cells. The magnetic dipole-dipole interaction f_d is given by[20]

$$f_d=\frac{1}{2}g_d|\hat{\mathbf{d}}\times\hat{\mathbf{l}}|^2. \tag{16}$$

The magnetic anisotropy term is

$$f_h=\frac{1}{2}g_h(\hat{\mathbf{d}}\cdot\mathbf{H})^2, \tag{17}$$

and the gradient energy[21]

$$\begin{aligned}2f_g=&\rho_\perp\mathbf{v}^2+(\rho_\parallel-\rho_\perp)(\hat{\mathbf{l}}\cdot\mathbf{v})^2+2C\mathbf{v}\cdot\nabla\times\hat{\mathbf{l}}\\&-2C_0(\hat{\mathbf{l}}\cdot\mathbf{v})(\hat{\mathbf{l}}\cdot\nabla\times\hat{\mathbf{l}})+K_s(\nabla\cdot\hat{\mathbf{l}})^2+K_t(\hat{\mathbf{l}}\cdot\nabla\times\hat{\mathbf{l}})^2\\&+K_b|\hat{\mathbf{l}}\times(\nabla\times\hat{\mathbf{l}})|^2+K_5|(\hat{\mathbf{l}}\cdot\nabla)\hat{\mathbf{d}}|^2\\&+K_6\sum_{ij}[(\hat{\mathbf{l}}\times\nabla)_i\hat{\mathbf{d}}_j]^2.\end{aligned} \tag{18}$$

The gradient term includes also the kinetic energy, which is a function of the counterflow velocity $\mathbf{v}=\mathbf{v}_s-\mathbf{v}_n$. It follows from the structure of the functional that $F_{\text{eq}}(H,\Omega)$ of the equilibrium state is a nondecreasing function of both H and Ω. The zero of the energy is chosen so that $F_{\text{eq}}(H,0)=0$.

It should be noted that $\mathbf{v}_s$ and $\hat{\mathbf{l}}=\hat{\mathbf{m}}\times\hat{\mathbf{n}}$ are not completely independent variables but are constrained by the Mermin-Ho relation (13). In order to avoid such complicated constraints, we use $\hat{\mathbf{d}}$, $\hat{\mathbf{m}}$, and $\hat{\mathbf{n}}$ as the basic variables. With these variables the constraints are simpler: $\hat{\mathbf{d}}$, $\hat{\mathbf{m}}$, and $\hat{\mathbf{n}}$ have to be unit vectors and $\hat{\mathbf{m}}\perp\hat{\mathbf{n}}$. The energy functional (15) can be expressed as a function of $\hat{\mathbf{d}}$, $\hat{\mathbf{m}}$, and $\hat{\mathbf{n}}$. Only the gradient terms require some calculation, and we get

$$2f_g=(\overline{\rho_\parallel}+2K_7)\sum_i(\hat{\mathbf{m}}\cdot D_i\hat{\mathbf{n}})^2+(K_s+K_7)\sum_i[(\hat{\mathbf{m}}\cdot\mathbf{D}\hat{m}_i)^2+(\hat{\mathbf{n}}\cdot\mathbf{D}\hat{n}_i)^2]+2K_s\sum_i(\hat{\mathbf{m}}\cdot\mathbf{D}\hat{m}_i)\hat{\mathbf{n}}\cdot\mathbf{D}\hat{n}_i$$

$$+(K_t+K_7)\sum_i[(\hat{\mathbf{n}}\cdot\mathbf{D}\hat{m}_i)^2+(\hat{\mathbf{m}}\cdot\mathbf{D}\hat{n}_i)^2]-2K_t\sum_i(\hat{\mathbf{n}}\cdot\mathbf{D}\hat{m}_i)\hat{\mathbf{m}}\cdot\mathbf{D}\hat{n}_i+(K_b+\overline{C}-\overline{C_0}+K_7)[(\mathbf{D}\cdot\hat{\mathbf{m}})^2+(\mathbf{D}\cdot\hat{\mathbf{n}})^2]$$

$$+2(K_b-\overline{C_0}+K_7)\sum_i[(\mathbf{D}\cdot\hat{\mathbf{m}})\hat{m}_i\hat{\mathbf{n}}\cdot\mathbf{D}\hat{n}_i-(\mathbf{D}\cdot\hat{\mathbf{n}})\hat{m}_i\hat{\mathbf{m}}\cdot\mathbf{D}\hat{n}_i]+(\overline{C_0}-\overline{C})\sum_{ik}[(D_i\hat{m}_k)D_k\hat{m}_i+(D_i\hat{n}_k)D_k\hat{n}_i]$$

$$-K_7\sum_{ik}[(D_i\hat{m}_k)^2+(D_i\hat{n}_k)^2]+K_5\sum_{ik}(\nabla_i\hat{d}_k)^2+(K_6-K_5)\sum_i[(\hat{\mathbf{m}}\cdot\boldsymbol{\nabla}\hat{d}_i)^2+(\hat{\mathbf{n}}\cdot\boldsymbol{\nabla}\hat{d}_i)^2]. \tag{19}$$

Here we use gauge-invariant derivatives $\mathbf{D}\hat{m}_i=\boldsymbol{\nabla}\hat{m}_i+\tilde{\mathbf{v}}_n\hat{n}_i$ and $\mathbf{D}\hat{n}_i=\boldsymbol{\nabla}\hat{n}_i-\tilde{\mathbf{v}}_n\hat{m}_i$. We have also used the notations $\tilde{\mathbf{v}}_n=(2m_3/\hbar)\boldsymbol{\Omega}\times\mathbf{r}$, $\overline{\rho}=(\hbar/2m_3)^2\rho$, $\overline{C}=(\hbar/2m_3)C$, and $K_7=\overline{\rho_\perp}-\overline{\rho_\parallel}-K_s-K_t+K_b-2\overline{C_0}$.

One can transform the gradient energy (19) by partial integration. For example, $\int d^3r(\nabla_i\hat{m}_k)\nabla_k\hat{m}_i=\int d^3r(\boldsymbol{\nabla}\cdot\hat{\mathbf{m}})^2$ plus a surface term. For the present purposes such partial integrations can be done without paying attention to the surface terms. The reasons are that (i) the surface terms can affect the equilibrium configuration only near surfaces, if anywhere, and (ii) although the local energy density is changed in the partial integration, all the energies of vortices are unchanged because of the periodic boundary conditions.

The full gradient energy (19) is written down here in order to demonstrate that our calculational method is feasible whenever the hydrodynamic approximation is valid. In particular, the theory applies to all temperatures $T<T_c$ except a small region near T_c (due to the A_1 phase) and another region around $T=0$. However, the present numerical calculations are made in the Ginzburg-Landau (GL) region.[17] This means temperatures only near T_c ($T_c-T\ll T_c$), but this range is still wider than the one that has to be excluded because of distortion towards the A_1 phase. In this region the GL theory is more general than the hydrodynamic one. If one makes the hydrodynamic approximation in the GL theory, one arrives at the set of equations presented above, but with certain restrictions on the coefficients. They are $\overline{\rho_\parallel}/2=\overline{\rho_\perp}/(\gamma+1)=\overline{C}/(\gamma-2\eta)=\overline{C_0}/(\gamma-1)=K_s=K_t=K_b/\gamma=K_5/2=K_6/(\gamma+1)$. These conditions imply that all terms that are higher than second order in $\hat{\mathbf{m}}$ or $\hat{\mathbf{n}}$ disappear from the gradient energy (19).

Collecting all simplifications and reducing units, we can write the energy terms as

$$f_d=\frac{1}{2}[(\hat{\mathbf{d}}\cdot\hat{\mathbf{m}})^2+(\hat{\mathbf{d}}\cdot\hat{\mathbf{n}})^2]$$

$$f_h=\frac{1}{2}(\hat{\mathbf{d}}\cdot\mathbf{H})^2,$$

$$4f_g=\sum_{ik}[\nabla_i\hat{m}_k+(v_n)_in_k]^2+\sum_{ik}[\nabla_i\hat{n}_k-(v_n)_im_k]^2$$

$$+(\gamma-1)\Big[(\boldsymbol{\nabla}\cdot\hat{\mathbf{m}}+\mathbf{v}_n\cdot\hat{\mathbf{n}})^2+(\boldsymbol{\nabla}\cdot\hat{\mathbf{n}}-\mathbf{v}_n\cdot\hat{\mathbf{m}})^2$$

$$+\sum_i(\hat{\mathbf{m}}\cdot\boldsymbol{\nabla}\hat{d}_i)^2+\sum_i(\hat{\mathbf{n}}\cdot\boldsymbol{\nabla}\hat{d}_i)^2\Big]+2\sum_{ik}(\nabla_i\hat{d}_k)^2$$

$$+4(2\eta-1)\mathbf{m}\times\mathbf{n}\cdot\boldsymbol{\Omega}, \tag{20}$$

where $\mathbf{v}_n=\boldsymbol{\Omega}\times\mathbf{r}$. We have used ''dipole units'' for length $[\xi_d=(\hbar/2m_3)\sqrt{\rho_\parallel/g_d}]$, field $(H_d=\sqrt{g_d/g_h})$, angular velocity $(\Omega_d=\hbar/2m_3\xi_d^2)$, and energy density (g_d).

It should be noted that the functional (20) is based on purely phenomenological considerations. These leave open only two dimensionless parameters γ and η. (In the notation of Ref. 22, $\gamma=K_L/K_T$ and $\eta=K_C/K_T$.) They can be calculated in the quasiclassical theory. In the weak-coupling approximation $\gamma=3$ and $\eta=1$. A more complicated weak-coupling-plus model gives $\gamma\approx3.1$, but η is unchanged.[22] We have made a few tests that our results are not sensitive to the value of γ, so we will use the weak-coupling values in the following.

IV. NUMERICAL CALCULATION

For numerical computation the energy functional (20) was discretized on a lattice. We assume that there is no dependence on z, so that a two-dimensional square lattice (x_j,y_k) is sufficient. The first thing in the numerical program is to specify the magnetic field, the rotation velocity Ω, the circulation number N and the Bravais lattice. For rectangular lattices one needs to specify the ratio b/a, where a denotes the length of the shortest possible primitive vector, and b is the lattice constant in the perpendicular direction in the rectangular cell. No oblique lattices were found. The area of the primitive cell was then determined from Eq. (6). For simplicity of boundary conditions, it was useful to choose the lattice constant of the calculational lattice commensurate with the primitive cell of the vortex lattice. The last preparatory step was to give an initial guess for the fields $\hat{\mathbf{d}}$, $\hat{\mathbf{m}}$, and $\hat{\mathbf{n}}$. Then the values $\hat{\mathbf{d}}(x_j,y_k)$, $\hat{\mathbf{m}}(x_j,y_k)$, and $\hat{\mathbf{n}}(x_j,y_k)$ were changed iteratively. At each lattice point (x_j,y_k) in the primitive cell, a torque acting on the spin vector $(\hat{\mathbf{d}})$ and on the orbital vectors ($\hat{\mathbf{m}}$ and $\hat{\mathbf{n}}$) was calculated, and the vectors were rotated proportionally to the torque.[23] The proportionality coefficient was chosen experimentally to achieve fast conver-

gence. The values of the fields outside the primitive cell were determined from the periodic boundary conditions (3) and (4). As discussed above, the coefficients C_1 and C_2 are arbitrary but it was natural to choose them consistent with the initial guess in order to avoid unnecessary motion of the vortex. We assume $C_3=0$. The iteration was continued until the energy converged, and the torques approached zero.

For rectangular lattices, the energy F needs to be minimized also with respect to the ratio of the lattice constants $u=b/a$. This process is considerably simplified by noting that a calculation at a given value of u not only gives $F(u)$, but also the first derivative $dF(u)/du$ at constant area ab. It follows from the stationarity of the energy functional that

$$\frac{dF(u)}{du}=\frac{1}{2uV}\int_V d^3r\sum_{ij}\left(\frac{\partial f_{\rm g}}{\partial D_x A_{ij}}D_x A_{ij} - \frac{\partial f_{\rm g}}{\partial D_y A_{ij}}D_y A_{ij}+\text{c.c.}\right). \tag{21}$$

Here A_{ij} is the general order-parameter matrix in superfluid ^{3}He and c.c. the complex conjugate. Application to functional (20) gives

$$\frac{dF(u)}{du}=\frac{1}{uV}\int_V d^3r(T_x-T_y), \tag{22}$$

where

$$\begin{aligned}4T_i=&\sum_k(\nabla_i\hat{m}_k+v_{{\rm n}i}\hat{n}_k)^2+\sum_k(\nabla_i\hat{n}_k-v_{{\rm n}i}\hat{m}_k)^2+(\gamma-1)\\&\times\Big[(\nabla_i\hat{m}_i+v_{{\rm n}i}\hat{n}_i)(\boldsymbol{\nabla}\cdot\hat{\mathbf{m}}+\mathbf{v}_{\rm n}\cdot\hat{\mathbf{n}})+(\nabla_i\hat{n}_i-v_{{\rm n}i}\hat{m}_i)\\&\times(\boldsymbol{\nabla}\cdot\hat{\mathbf{n}}-\mathbf{v}_{\rm n}\cdot\hat{\mathbf{m}})+\sum_k(\hat{m}_i\nabla_i\hat{d}_k)\hat{\mathbf{m}}\cdot\boldsymbol{\nabla}\hat{d}_k\\&+\sum_k(\hat{n}_i\nabla_i\hat{d}_k)\hat{\mathbf{n}}\cdot\boldsymbol{\nabla}\hat{d}_k\Big]+2\sum_k(\nabla_i\hat{d}_k)^2.\end{aligned} \tag{23}$$

The iteration was often started with a rather small number of lattice points ($\sim$1000), and this was iterated to convergence. Then new lattice points were added in between the old ones, and the iteration was continued. The maximum final lattices contained around 100 000 points.

The procedure was repeated for several different initial guesses and values of magnetic field and rotation velocity. Although the finding of the minimum-energy structures is a well defined mathematical problem, physical intuition is needed in inventing the initial guesses. Particularly good guesses are the models used in previous investigations of vortices. In addition, we tried several variants of these. The initial guesses leading to the different structures are listed in the Appendix.

V. RESULTS

In all calculations $T\approx T_{\rm c}$ and the field $\mathbf{H}$ was chosen parallel to the rotation axis z. The phase diagram of vortices in the plane formed by the magnetic field H and the rotation velocity Ω is shown in Fig. 1. There are six equilibrium

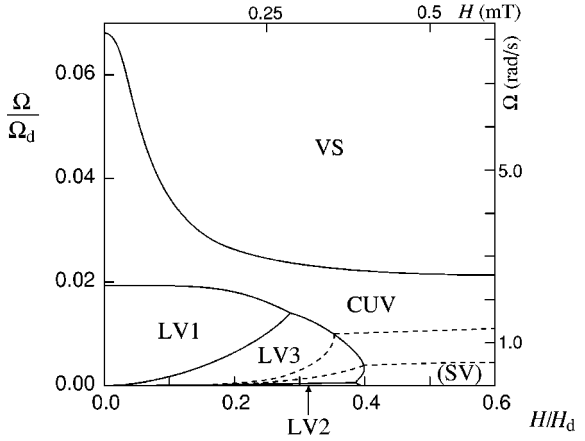

FIG. 1. The phase diagram of vortices in the plane formed by the magnetic field $\mathbf{H}$ and the rotation velocity $\boldsymbol{\Omega}\|\mathbf{H}$. The calculation is done using the dimensionless units given below Eq. (20). The solid lines denote phase boundaries between different continuous vortices [locked vortices (LV1, LV3), continuous unlocked vortex (CUV), and vortex sheet (VS)]. The LV2 should become the equilibrium locked vortex at very low $\Omega\lesssim 0.0005\Omega_{\rm d}$. The dashed lines denote the phase boundaries of the singular vortex (SV) against the LV3 and the CUV. These are calculated using two values of the SV energy parameter: $c=2.6$ (upper dashed line) and $c=3.1$ (lower dashed line). The real units for Ω and H are calculated using $\Omega_{\rm d}=120$ rad/s and $H_{\rm d}=2.0$ mT, which are estimated for the pressure of 29 bars.

vortex types, which are discussed separately below. In the names of the vortices, we follow Ref. 1. The energy densities F (15) of the vortices are expressed in reduced units defined under Eq. (20). We chose the x axis parallel to the shortest primitive vector of the two-dimensional Bravais lattice.

(i) The locked vortex 1 (LV1) has the quantum numbers $N=4$ and $\nu_l=\nu_d=2$.[14,24–28] Its most distinguishing feature is the square Bravais lattice. The space group is $P(4/n)(2'/b')(2'/m')$, or shortly, $P4/nb'm'$. The symmetry operations of this as well as other space groups are listed in Ref. 10.

Qualitatively the structure can be understood so that the first thing to minimize is the dipole energy (16). This gives a ''locked'' configuration where $\hat{\mathbf{d}}=\hat{\mathbf{l}}$ everywhere. If the field is zero, then the energy of this structure arises solely from the gradient terms (18). These are minimized by a smooth distribution where the gradient of $\hat{\mathbf{l}}$ has the same order of magnitude everywhere. Numerical calculations show that this is achieved in a square lattice with $N=4$; see Fig. 2.

The structure can be interpreted to consist of four elementary units. These units are called Mermin-Ho vortices because of a resembling structure first described in a cylindrical container.[19] The boundary of each unit can be defined by $\hat{l}_z=0$. Two of the four units have a circular distribution of $\hat{\mathbf{l}}$ and $\hat{l}_z>0$ ($\hat{\mathbf{l}}\cdot\boldsymbol{\Omega}>0$). The other two have a hyperbolic distribution and $\hat{l}_z<0$. It follows from Eq. (13) that each elementary vortex contributes a unity to $N=4$. A finite axial field makes the cores of the Mermin-Ho vortices shrink because the field favors the orientation $\hat{\mathbf{d}}\perp\hat{\mathbf{z}}$ at the borders of the elementary vortices.

At $H=0$ we find the energy $F=4.72\Omega^{0.997}$ in the range $\Omega=0.005-0.04$. In the case of perfect locking ($\hat{\mathbf{d}}\equiv\hat{\mathbf{l}}$), the

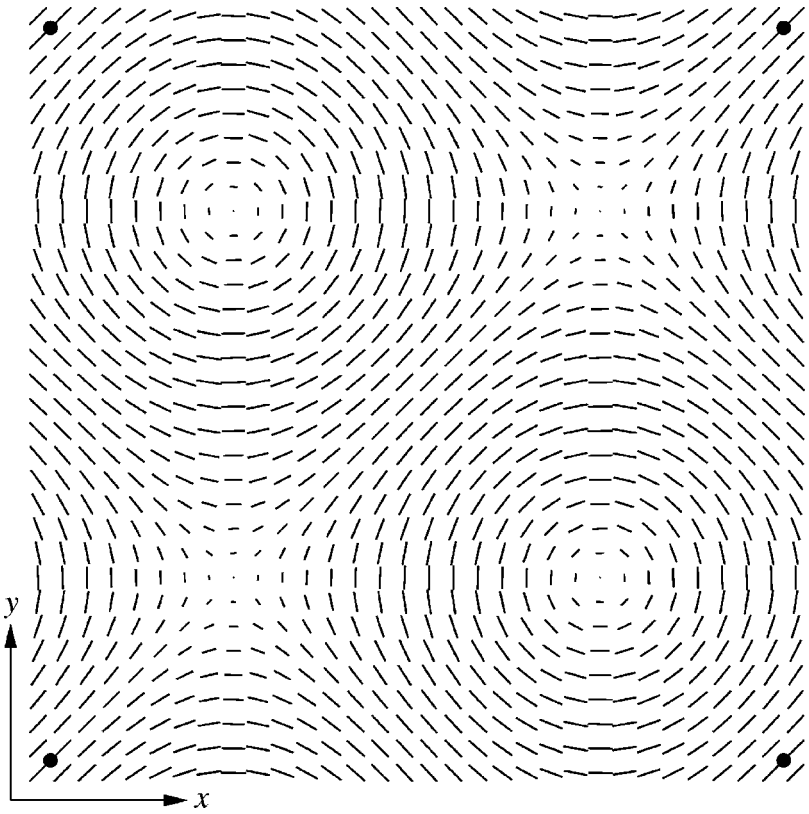

FIG. 2. Locked vortex 1 (LV1) in zero field. In Figs. 2–6, the short lines denote the projection of the unit vector $\hat{\mathbf{l}}$ to the $x-y$ plane. For clarity of figure, the heads of the arrows are omitted. The component $\hat{l}_z$ is positive ($\hat{\mathbf{l}}\cdot\mathbf{\Omega}>0$) in regions where $(\hat{l}_x,\hat{l}_y)$ has circular appearance, and negative in regions where $(\hat{l}_x,\hat{l}_y)$ is hyperbolic. The dots denote equivalent points in the periodic lattice. The LV1 has the square Bravais lattice and the space group $P4/nb'm'$.

energy would be strictly linear in Ω. We find that this is only an approximation because with increasing Ω the kinetic energy (18) is reduced at the expense of the dipole energy (16). Our energy can be compared with Ref. 14, where a variational calculation gives a 30% and a model based on isolated Mermin-Ho vortices a 6% larger value.

A possible competitor to the LV1 structure is a hexagonal lattice with $N=2\nu_l=2\nu_d=2$.[29] The ansatz form has $\hat{\mathbf{l}}\|\mathbf{\Omega}$ at the borders of the Wigner-Seitz cell. The space group is either $P6m'm'$ for a radial and $P62'2'$ for a circular distribution of $\hat{\mathbf{l}}$. In agreement with previous authors, we find that this structure does not correspond to the minimum energy at any values of Ω and H.[14,25,28]

(ii) The locked vortex 3 (LV3) has the same quantum numbers $N=4$ and $\nu_l=\nu_d=2$ as LV1. The main difference is that the lattice structure is primitive rectangular rather than a square. The space group is $P(2'/b')(2'/a')(2/n)$, or shortly $Pb'a'n$. This structure has not been previously studied in the literature.

The LV3 structure can be understood as a modification of the LV1 structure. When the cores of the Mermin-Ho vortices shrink with increasing magnetic field, there remains a large bending of $\hat{\mathbf{d}}\approx\hat{\mathbf{l}}$ outside of the cores. The gradient energy in this region can be reduced by rearranging the Mermin-Ho vortices. In LV3 the Mermin-Ho vortices form infinite chains, as visible in Fig. 3. The chains, or sheets consist of alternating circular and hyperbolic units. Outside the sheets, the $\hat{\mathbf{d}}\approx\hat{\mathbf{l}}$ fields are nearly constant and parallel (or antiparallel) to x.

In contrast to all other vortex transitions, the change between LV1 and LV3 seems to be of the second order. The lattice ratio b/a grows continuously from unity at the transition. At constant H, the b/a ratio grows with decreasing Ω and reaches 3.4 at our lowest $\Omega=0.001$ at $H=0.6$. We fit $F=\Omega(3.62+0.37\Omega^{-0.36})$ at $H=0.3$ in the range $\Omega=0.001-0.008$. Here all three parameters are free in the fit.

It was demonstrated by Fujita and Ohmi that the LV1 is unstable to a deformation.[30] They found a structure where four Mermin-Ho vortices form a unit that is separated by some distance from the other units. We find that this structure has higher energy than the LV3.

(iii) The locked vortex 2 (LV2) (Ref. 27) is defined by $N=2$ and $\nu_l=\nu_d=1$. The space group is $C12'1$, or shortly, $C2'$, where C denotes the centering of the rectangular lattice. The LV2 represent an alternative deformation of the LV1 when the cores of the elementary vortices shrink in increasing magnetic field. Here the Mermin-Ho vortices form pairs. Each pair consists of one circular and one hyperbolic unit; see Fig. 4. Outside such a pair, the $\hat{\mathbf{d}}\approx\hat{\mathbf{l}}$ fields are nearly constant and parallel to x. This special direction breaks the hexagonal lattice symmetry, which otherwise could apply to such well separated vortices. Therefore we expect the lattice structure is centered rectangular. We find that the ratio of the two lattice constants $b/a\approx1.8$. This is less than $b/a=\sqrt{6}$, which is obtained from the hexagonal lattice (having $b/a=\sqrt{3}$) by scaling x and y according to the anisotropy of the superfluid density ($\rho_\perp=2\rho_\parallel$).

The LV2 has only one point symmetry $2'_y$, which means a rotation by π around the y axis combined with time inversion. In previous ^{3}He literature the $2'$ symmetry was denoted by w.[6] The symmetry implies that $\hat{d}_y$ and $\hat{l}_y$ change signs when $x\rightarrow-x$ in Fig. 4, and other components of $\hat{\mathbf{d}}$ and $\hat{\mathbf{l}}$ remain unchanged. The symmetry transformation of $\hat{\mathbf{m}}$ and $\hat{\mathbf{n}}$ depends on the specific choice of the phase factors.

The LV2 is doubly degenerate. The degenerate forms are

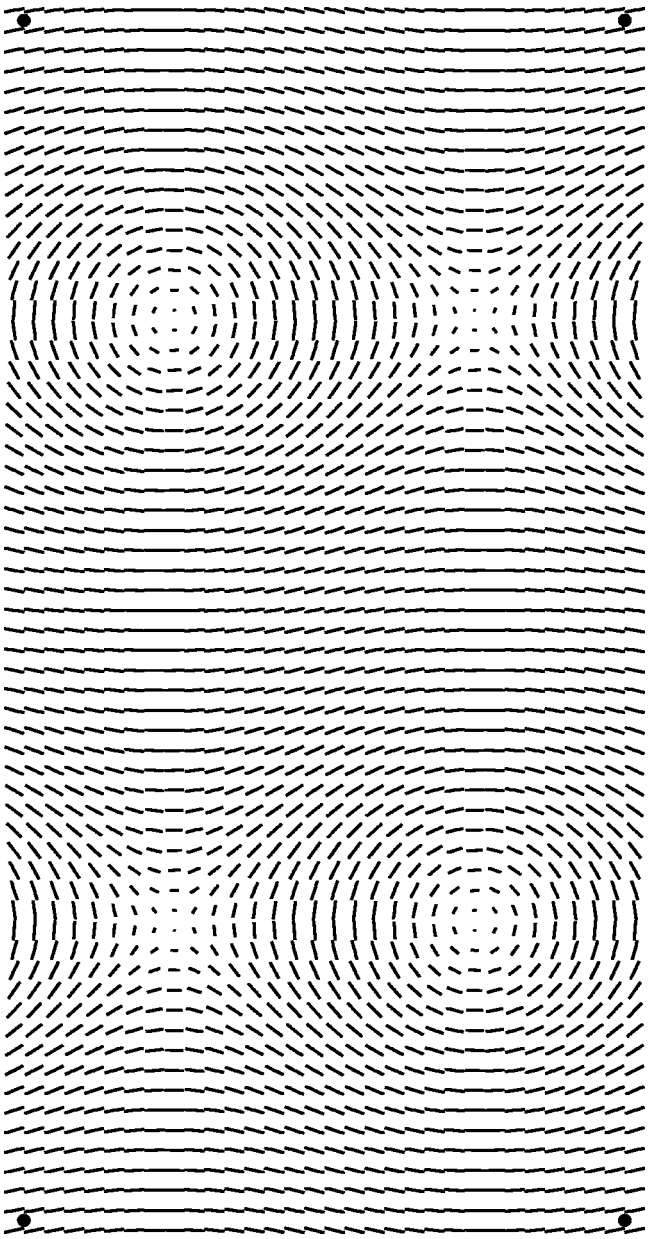

FIG. 3. Locked vortex 3 (LV3) for $H=0.3H_{\rm d}$ and $\Omega=0.006\Omega_{\rm d}$. The notation is the same as in Fig. 2. The LV3 has the primitive rectangular Bravais lattice and the space group $Pb'a'n$. The spacing of the plotted $\hat{\mathbf{l}}$ vectors is $1.08\xi_{\rm d}$.

obtained from each other by exchanging the positions of the circular and hyperbolic Mermin-Ho vortices. Formally this can be done by the operation m_y'. In the calculation we have only studied the simplest case where all LV2 vortices have the same orientation. If both degenerate forms are present simultaneously, it would lead to a larger primitive cell or, in an extreme case, absence of periodicity.

We find the energy $F=\Omega[-1.14+1.37\ln(1/\Omega+1/0.00412)]$ at $H=0.3$ in the range $\Omega=0.001-0.008$. In this fit we kept the constant 1.37 multiplying the logarithm fixed. This constant arises from the flow far from the vortex cores, and it should become exact in the limit $\Omega\to 0$. The numerical value 1.37 is calculated in Ref. 31. The constant -1.14 can be interpreted as the core energy of the vortex line. The constant 0.004 12 describes the angular velocity

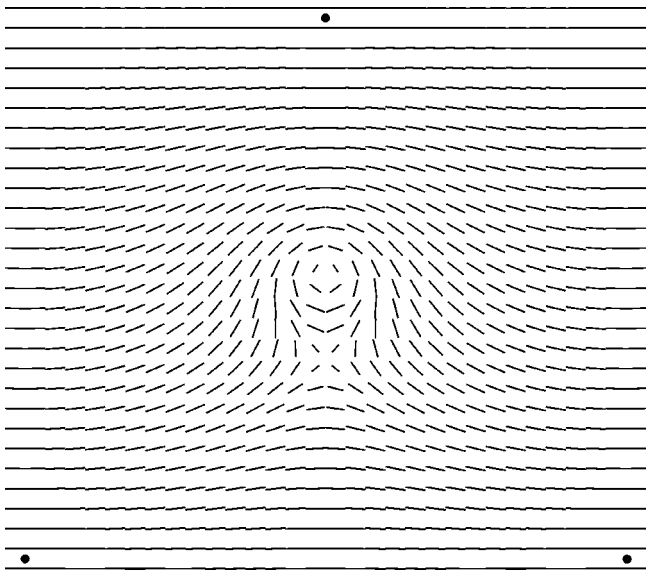

FIG. 4. Locked vortex 2 (LV2) for $H=0.4H_{\rm d}$ and $\Omega=0.002\Omega_{\rm d}$. The notation is the same as in Fig. 2. The LV2 has the centered rectangular Bravais lattice and the space group $C2'$. The spacing of the plotted $\hat{\mathbf{l}}$ vectors is $1.97\xi_{\rm d}$.

where the cores of the vortices start to overlap. In the range of our calculation the LV2 has higher energy than LV3. However, it is expected that the LV2 becomes absolutely stable in the limit $\Omega\to 0$. Extrapolating the expressions of the energies we can estimate that this takes place at $\Omega\lesssim 0.0005$.

(iv) The continuous unlocked vortex (CUV) has $N=2$, $\nu_l=1$, and $\nu_d=0$.[26–28,32–40] The space group is $C2'$. The CUV is similar to the LV2 with respect to N, ν_l, and the space group, see Fig. 5. The crucial difference compared to

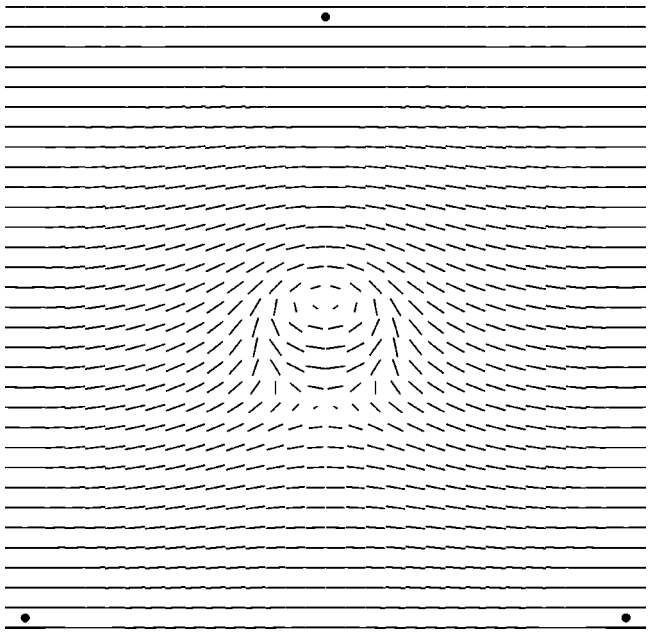

FIG. 5. Continuous unlocked vortex (CUV) for $H=0.3H_{\rm d}$ and $\Omega=0.02\Omega_{\rm d}$. The notation is the same as in Fig. 2. Similar to LV2, the CUV has the centered rectangular Bravais lattice and the space group $C2'$. The spacing of plotted $\hat{\mathbf{l}}$ vectors is $0.59\xi_{\rm d}$.

the LV2 is that ν_d vanishes. Vortices where $\hat{\mathbf{d}}$ and $\hat{\mathbf{l}}$ differ essentially from each other ($\nu_d \neq \nu_l$) are called ''unlocked.''

The principle in all unlocked vortices is to minimize the field energy (17) in the first place, and therefore they are more economical in large fields $H \gtrsim H_{\mathrm{d}}$ than the locked structures. In the CUV, $\hat{\mathbf{d}}$ is approximately constant and parallel to x everywhere. The region where $\hat{\mathbf{d}}$ and $\hat{\mathbf{l}}$ differ from each other is called a ''soft core.'' Its size $\sim \xi_{\mathrm{d}}$ is determined by the balance of the kinetic energy of $\mathbf{v}$ (18) outside of the soft core and the dipole energy (16) inside. (Note that the total gradient energy of $\hat{\mathbf{l}}$ in the core is approximately independent of the size.)

The first suggestion for CUV had the m' symmetry.[32] Similar to several previous calculations, we find that the $2'$ symmetric form has a lower free energy at all values of Ω and H.[33,36,38,40] The m' symmetric form seems to correspond to a saddle point of the free energy.

Similar to the LV2, the CUV probably has the centered rectangular lattice, and we find that $b/a \approx 2$. The energy of the CUV depends surprisingly much on the magnetic field. At $H=0$ we fit $F=\Omega[-0.728+1.37\ln(1/\Omega+1/0.219)]$ but at $H=0.6$ we find $F=\Omega[-0.591+1.37\ln(1/\Omega+1/0.0894)]$. The expressions are most accurate in the range $\Omega=0.008-0.03$. Similar to the LV2, the value 1.37 is kept fixed in fitting the two other parameters. The interpretation of the other parameters is the same as for LV2. The curving of the phase boundary between CUV and VS (Fig. 1) arises from the field dependence of CUV, as VS seems to be rather insensitive to H.

According to our earlier calculation, the transition between the CUV and the LV2 takes place at $H=0.4$ in the limit $\Omega \to 0$.[23] This agrees with the present calculation. We find the triple point between the LV1, the LV3, and the CUV at $H=0.29$ and $\Omega=0.014$.

(v) The vortex sheet (VS) has $N=4$, $\nu_l=2$, and $\nu_d=0$.[41,9,42] The likely space group is $Pb'a'n$, similar to the LV3. Here N, ν_l, and ν_d are all the same as for the CUV except multiplication by 2. The crucial difference between the VS and the CUV becomes evident when their primitive cells are stacked one after another: in the CUV the soft cores form a two-dimensional lattice of lines while in the VS they form a series of equidistant planes parallel to x; see Fig. 6. The $\hat{\mathbf{d}}$ vector is approximately constant and parallel to $\hat{\mathbf{x}}$ everywhere.

The close similarity of the CUV and the VS is illuminated if one thinks bending a VS and closing it to a cylinder. The CUV represents the smallest among such cylinders because it contains just one periodic unit of a vortex sheet. This relationship is also evident in the ansatz forms given in the Appendix.

We have discussed above how the LV1 is transformed to the LV2 by pairing the Mermin-Ho units. Then the CUV evolved from the LV2 when the dipole locking was removed. After that the VS was developed by opening the cylindrical structure of the CUV. We can now return to the starting point by noting that forcing dipole locking in the VS gives the structure of LV1 and LV3. The close similarity of the VS and the LV3 is evident from the symmetry groups and from Figs. 2 and 3.

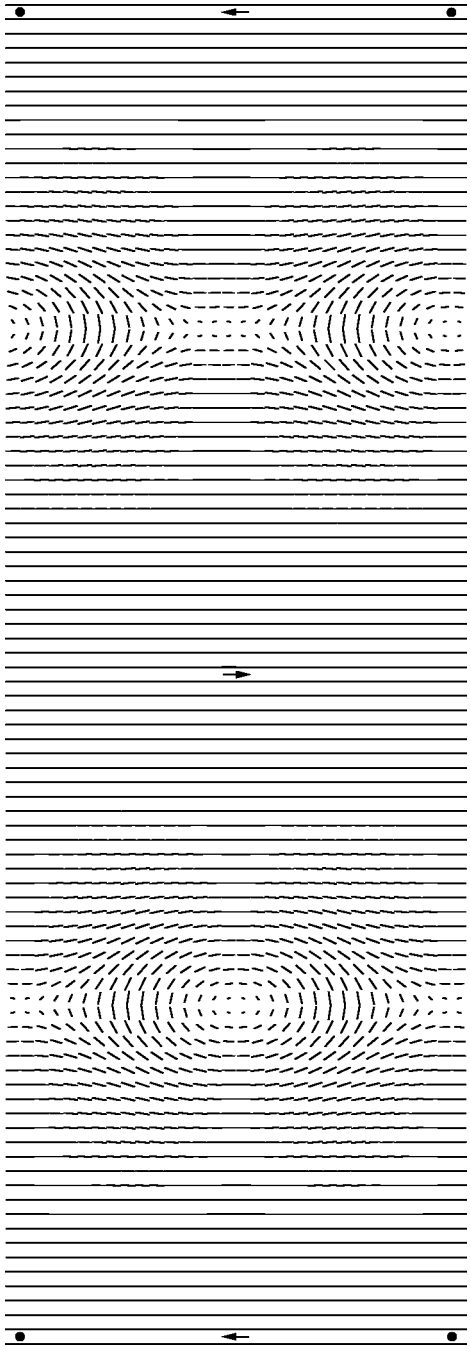

FIG. 6. Vortex sheet (VS) for $H=0.2H_{\mathrm{d}}$ and $\Omega=0.03\Omega_{\mathrm{d}}$. The notation is the same as in Fig. 2. The VS has the primitive rectangular Bravais lattice and the space group $Pb'a'n$. The primitive cell contains two vortex sheets parallel to x. The arrows denote the opposite directions of $\hat{\mathbf{l}}$ on different sides of the sheets. The spacing of plotted $\hat{\mathbf{l}}$ vectors is $0.39\xi_{\mathrm{d}}$.

The $\hat{\mathbf{l}}$ vector in the VS is approximately parallel to x outside of the soft cores, but it has opposite directions on the two sides of the sheet. This implies that the primitive cell must contain (at least) two neighboring sheets. This is the reason for the double size of the primitive cell compared to the simplest lattice structure of the CUV. The surface tension of the sheet makes the primitive cell rather short in the x direction. We note that the present definition of b according to the primitive rectangular Bravais lattice is twice as large

as in Refs. 9, 41, and 42, where b denotes the distance between neighboring sheets. Because the sheets are far from each other, the sliding of the sheets relative to each other probably leads to a negligible change in the energy.

The properties of the VS depend very weakly on the magnetic field in the studied region $H \leqslant 0.6$. The results of our calculations can be represented by $b/a = 1.26\Omega^{-0.255}$ and $F = 1.35\Omega^{0.664}$ for $\Omega = 0.016$–0.07. Both these quantities are slightly larger than obtained from the twist-section model,[9] which gives $b/a = (1/\pi)(18/\Omega)^{1/3}$ and $F = \frac{1}{2}(18\Omega^2)^{1/3}$. The uniform winding model is a slightly more complicated variational ansatz.[9,42] It gives an upper bound for the energy that is 10% higher at $\Omega = 0.016$ and 3% higher at $\Omega = 0.07$. In the limit $H \gg 1$ we find the transition between CUV and VS at $\Omega = 0.022$.

An interesting feature in the phase diagram is that both the CUV and the VS are stable also in zero field. Although it has not been stated explicitly, the crossing of the energies of the LV1 and the CUV at $H = 0$ appears also in previous literature. Comparison of the energies given in Refs. 14 and 40, for example, gives it at $\Omega = 0.023$. It was calculated in Ref. 25 that there is a transition from the LV1 to a singular $\hat{z}$ vortex when $\Omega = 0.11$. This prediction has to be revised because both the CUV and the VS have a much lower energy at this rotation velocity. If there is a transition to the $\hat{z}$ vortex, it takes place at a much higher Ω than expected in Ref. 25.

The energy difference of the CUV and the VS relative to the LV1 at $H = 0$ arises from competition of the dipole energy and the gradient energy of $\hat{\mathbf{d}}$. The LV1 is stable at a low Ω because the dipole energy is minimized in the first place, and the gradient energy associated with $\hat{\mathbf{d}}$ is not important. With increasing Ω the gradient energy becomes larger. At the transition point, it becomes more economic to arrange $\hat{\mathbf{d}}$ approximately constant although it means increased dipole energy in the soft core of the CUV or the VS. Based on purely dimensional considerations, this transition was expected at $\Omega \sim 1$ ($\Omega \sim \Omega_d \approx 120$ rad/s in real units).[14] However, the present calculation gives the transition between the CUV and the LV1 at $\Omega = 0.019$, which is almost two orders of magnitude smaller than the naive expectation.

(vi) The singular vortex (SV) has $N = 1$ and the space group $C1m'1$, or shortly Cm'.[32,34,40] No other vortex considered here has $N = 1$ because it is not possible for the continuous vortices as a result of Eq. (14). The Ω dependence of the energy can be written $F = \Omega[c(H,T) - 0.70 \ln \Omega]$ at small Ω. Here the factor 0.70 arises from the flow field far from the vortex line.[31] This factor is approximately one half of the value for a $N = 2$ vortex line. Therefore the singular vortex is favored over the CUV at a low Ω.

Based on topological arguments alone, the structure of the singular vortex could be very simple. For example, $\hat{\mathbf{m}} + i\hat{\mathbf{n}} = \exp(i\phi)(\hat{\mathbf{y}} + i\hat{\mathbf{z}})$ and $\hat{\mathbf{d}} = \hat{\mathbf{l}}$ everywhere except at the singular ''hard core,'' where these quantities are not defined. Here ϕ is the azimuthal angle. However, energetics prefers a more complicated structure that has a soft core in addition to the hard core.[32] This is because a structure with radial $\hat{\mathbf{l}}$ and constant $\hat{\mathbf{m}} = \hat{\mathbf{z}}$ has lower energy than the simple vortex. Outside of the soft core, $\hat{\mathbf{d}}$ and $\hat{\mathbf{l}}$ are both nearly parallel to x.

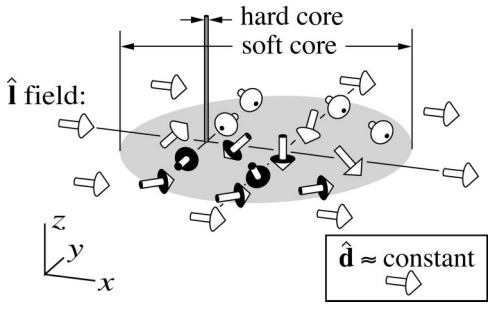

FIG. 7. Sketch of the core of the singular vortex (SV). The arrows denote $\hat{\mathbf{l}}$ and $\hat{\mathbf{d}}$. The soft core, where $\hat{\mathbf{d}}$ and $\hat{\mathbf{l}}$ differ considerably, appears as shaded.

Similar to the LV2 and the CUV, this gives rise to a centered rectangular lattice.

The hydrodynamic approximation used for the calculation of the continuous vortices is insufficient in the hard core of the SV. Therefore we have not calculated the function $c(H,T)$ in the energy F. Contrary to the continuous vortices, there is also a temperature dependence $c(H,T) \approx c(H) + 0.7 \ln(1 - T/T_c)$ because the size of the hard core depends on T. In order to get an idea of the complete phase diagram, the phase boundary of the SV is included in Fig. 1 (dashed lines) by two arbitrarily chosen constant values of $c(H,T)$.

The core structure of the SV can in principle be calculated using the Ginzburg-Landau theory, but there are two difficulties. First, this theory introduces additional parameters (such as the coefficients of the five energy terms that are of the fourth order in the order-parameter matrix) whose values are not well known. So the accuracy of the results would be less than in the hydrodynamic theory of continuous vortices. Second, the numerical calculation is difficult because the length scales associated with the soft ($\xi_d \approx 10\,\mu$m) and hard cores (≈ 10 nm) are very different.

We have made numerical simulations with Ginzburg-Landau theory where the difference in the soft- and hard-core scales is arbitrarily reduced. We cannot expect any quantitative results from such a calculation, but we believe that the following qualitative results are valid independently of our approximation. The structure around the hard core is

$$\pm\hat{\mathbf{l}} = \hat{\mathbf{y}} \sin\phi + \cos\phi(\hat{\mathbf{x}} \cos\eta + \hat{\mathbf{z}} \sin\eta), \tag{24}$$

where η is a constant angle, see Fig. 7 for illustration. The original suggestion[32] has $\eta = \pi/2$ whereas the minimum energy of the structure (24) prefers $\eta = 0$.[6] The true structure is likely to fall between these limits because $\eta = 0$ would imply a large gradient energy (18) in matching the hard core (24) with the constant $\hat{\mathbf{l}}$ outside of the soft core.

There is no circulation around the hard core. Thus all the circulation arises from the soft core, which is qualitatively described by the numbers $\nu_l = 1/2$ and $\nu_d = 0$. The centers of the hard and soft cores are displaced from each other in the x direction. The vortex has symmetry m_y', which in previous ^{3}He literature was called ν. In terms of the vectors this means that d_y and l_y change signs when $y \to -y$, and other components of $\hat{\mathbf{d}}$ and $\hat{\mathbf{l}}$ remain unchanged. The SV is doubly degenerate. The two forms are obtained from each other by the symmetry operation $2_y'$.

All the discussion above was for the case where the field **H** is parallel to **Ω**. As far as we know, other directions are considered only for the CUV (Refs. 39 and 35) and the VS.[42] Generally, it can be expected that the effect of field direction is not large in unlocked vortices, where $\hat{\mathbf{d}}$ is approximately constant, and thus f_h (17) can equally be minimized for arbitrary direction of **H**.

VI. COMPARISON WITH EXPERIMENTS

In order to compare the calculated phase diagram with measurements, one needs to know how to prepare the equilibrium state in experiments. This is not simple because the energy barriers separating the different vortex types are generally so large that it is difficult to induce any transitions.[1] So the decay of a metastable vortex type to the equilibrium type may be so slow that it cannot be observed. Also, if the rotation is started in the superfluid state, the vortex type that nucleates is generally not the equilibrium one. For example, only continuous vortices are nucleated if the rotation is started in the superfluid state; no singular vortex has been observed by this method.

The only exception to the above seems to be the region very near the superfluid transition temperature T_c. There the energy barriers separating the different vortex types are smallest. A practical way to perform the experiment is to cool slowly from the normal state ($T > T_c$) to the superfluid state at constant Ω and H. This procedure is expected to yield a state near the equilibrium one. It is important to remember, however, that the details of the transition in the presence of a thermal gradient and a magnetic field may be rather complicated.[1] Another limitation of the experiments is that they do not resolve the difference between the three types of the LV.

Also needed for the comparison are the values of Ω_d and H_d. We estimate $\Omega_d \approx 120$ rad/s, and $H_d \approx 2.0$ mT at 29 bars pressure. These are based on a weak-coupling analysis corrected by the enhancement of the energy gap according to Ref. 43. In addition, we have used the measured shift of the transverse NMR resonance frequency in the A (Ref. 44) or the B phase,[45] both of which give essentially the same result. The gap enhancement, which in Ref. 43 is given for the B phase as a function of the specific-heat jump ΔC_B, is applied to the A phase by replacing ΔC_B by $6/5\,\Delta C_A$.

The comparison of the experimental and theoretical phase diagrams is shown in Fig. 3 of Ref. 1. The qualitative agreement is good. A slight difference is that the vortex sheet is not observed in the experiments at the maximal angular velocity 3 rad/s although according to the present calculation it should show up above 2.6 rad/s, assuming $\Omega_d = 120$ rad/s. Possible explanations are that Ω_d is larger than we estimated or the cooling through T_c does not accurately produce the equilibrium state.

The six vortex types discussed above seem to be able to explain all the experiments that have been made in rotating bulk ^{3}He-A. We comment here on one controversial experiment. Torizuka *et al.*[46] observe a transition in the rotating state at $\Omega = 3$ rad/s when the rotation velocity was varied at constant $H = 0$. The original interpretation in the same reference postulated a layer of vortices on the container wall. We consider this interpretation unlikely because such a layer is probably unstable, as pointed out in Ref. 47. The present calculation now gives the possibility that the transition could be from the LV1 to either the CUV or the VS. Unfortunately, the collected experimental data does not seem sufficient to identify the structure at large Ω.[47,28]

VII. CONCLUSION

We have presented numerical calculations of the vortex structures in the Ginzburg-Landau region, and constructed a phase diagram in the $H-\Omega$ plane. There is in principle no difficulty in extending these calculations to lower temperatures. Although the phase diagram is not accessible experimentally at low temperatures, the calculation of the vortex structure would form the basis for a calculation of the NMR frequency shifts, which have been measured accurately.

Our search of vortex types was based on previous suggestions. There may well be structures which could not have evolved from the initial guesses we have used. In particular, only the simplest periodic structures were tested. From the experimental point of view, it seems that there is at present no need to introduce new types of vortices that are stable in bulk ^{3}He-A. That may change, however, when new regions are studied and more accurate measurements are done. In particular, low temperatures, high rotation velocities, high magnetic fields, the neighborhood of the A_1 phase, and restricted geometries could be studied. The studies could also be extended to metastable structures. For example, the LV was identified from its metastable modification in high field, which more appropriately should be classified as a different type of vortex.[1]

ACKNOWLEDGMENTS

We wish to thank A. Borovik-Romanov, P. Hakonen, M. Krusius, O. Nevanlinna, B. Plaçais, J. Simola, E. Sonin, and G. Volovik for useful discussions, and R. Hänninen for help in calculations.

APPENDIX

We give approximate expressions for the order parameter in different vortex structures. These can be used as initial guesses to produce the stable vortices discussed in Sec. V.

All structures can be simply represented using Euler angles (α, β, γ) but choosing x as the polar direction:

$$\hat{\mathbf{l}} = \hat{\mathbf{x}}\cos\beta + \sin\beta(\hat{\mathbf{y}}\cos\alpha + \hat{\mathbf{z}}\sin\alpha), \tag{A1}$$

$$\hat{\mathbf{m}} + i\hat{\mathbf{n}} = [-\hat{\mathbf{x}}\sin\beta + \cos\beta(\hat{\mathbf{y}}\cos\alpha + \hat{\mathbf{z}}\sin\alpha) + i(-\hat{\mathbf{y}}\sin\alpha + \hat{\mathbf{z}}\cos\alpha)]\exp(-i\gamma). \tag{A2}$$

In these coordinates the superfluid velocity (12) is

$$\tilde{\mathbf{v}}_s = -\boldsymbol{\nabla}\gamma - \cos\beta\boldsymbol{\nabla}\alpha. \tag{A3}$$

Depending on the vortex type, we present the Euler angles as functions of either rectangular (x, y, z) or cylindrical coordi-

nates (r, ϕ, z). Unless explicitly stated otherwise, the ansatz forms have the same symmetries as the vortices that they represent.

The VS has $\hat{\mathbf{d}}=\hat{\mathbf{x}}$ and $\alpha=-\gamma=\pi/2-2\pi x\,\mathrm{sgn}(y)/a$, where $\mathrm{sgn}(y)$ denotes the sign of y. β is a monotonic function of y so that $\beta(-b/2)=-\pi$, $\beta(0)=0$, and $\beta(b/2)=\pi$. Especially at low velocities this function is strongly nonlinear so that all the change of β takes place in narrow regions (thickness ~ 1) at the two vortex sheets, which are located at $y=\pm b/4$. This form of the order parameter is for a gauge where $\mathbf{v}_n=-2\Omega y\hat{\mathbf{x}}$. The transformation to the more usual gauge $\mathbf{v}_n=\mathbf{\Omega}\times\mathbf{r}$ is obtained by including an extra factor $\exp(i\Omega xy)$ multiplying the right-hand side of Eq. (A2). The lattice constants are constrained by $ab=4\pi/\Omega$ (6).

An approximation to LV1 and LV3 is the same as for VS except that $\hat{\mathbf{d}}=\hat{\mathbf{l}}$. The best guess for LV1 corresponds to $a=b$ and nearly linear $\beta(y)$. In spite of these choices, this Ansatz has less symmetry than the converged solution for LV1. A symmetric but more complicated Ansatz was suggested in Ref. 14. A third alternative is to glue together Ansatze of four Mermin-Ho vortices.

The CUV has $\hat{\mathbf{d}}=\hat{\mathbf{x}}$ and $\alpha=-\gamma=\phi$. β is a monotonic function of the radius r, which has $\beta(0)=0$ and $\beta(r)\approx\pi$ for $r>r_0$. Here the radius r_0 is of the order of a few units of length (ξ_d).

The LV2 is similar to CUV except that $\hat{\mathbf{d}}=\hat{\mathbf{l}}$. r_0 is of the order of H^{-1} in dimensionless units. The SV can be generated by $\hat{\mathbf{d}}=\hat{\mathbf{x}}$, $\gamma=0$, and $\alpha=\pi/2+\phi$. β is a monotonic function of r, which has $\beta(0)=\pi/2$ and $\beta(r)\approx\pi$ for $r>r_0$. Here r_0 is approximately unity. This Ansatz form has more symmetry than is present in a converged solution.

*Present address: Department of Physics, P.O. Box 9, 00014 University of Helsinki, Helsinki, Finland.

[1] Ü. Parts, J.M. Karimäki, J.H. Koivuniemi, M. Krusius, V.M.H. Ruutu, E.V. Thuneberg, and G.E. Volovik, Phys. Rev. Lett. **75**, 3320 (1995).

[2] E.V. Thuneberg, Czech. J. Phys. **46**, 2937 (1996).

[3] A.J. Leggett, Rev. Mod. Phys. **47**, 331 (1975).

[4] D. Vollhardt and P. Wölfle, *The Superfluid Phases of Helium 3* (Taylor & Francis, London, 1990).

[5] A.L. Fetter, in *Progress in Low Temperature Physics*, edited by D.F. Brewer (Elsevier, 1986), Vol. X, p. 1.

[6] M.M. Salomaa and G.E. Volovik, Rev. Mod. Phys. **59**, 533 (1987); **60**, 573(E) (1988).

[7] G.E. Volovik, *Exotic Properties of Superfluid ^3He* (World Scientific, Singapore, 1992).

[8] M. Krusius, J. Low Temp. Phys. **91**, 233 (1993).

[9] E.V. Thuneberg, Physica B **210**, 287 (1995).

[10] *International Tables for Crystallography*, edited by T. Hahn (D. Reidel Publishing, Dordrecht, 1983), Vol. A.

[11] W. Opechowski and R. Guccione, in *Magnetism*, edited by G.T. Rado and H. Suhl (Academic Press, New York, 1965), Vol. IIA.

[12] E. Brown, Phys. Rev. **133**, A1038 (1964).

[13] This mapping was used without explicit mention in Ref. 17 for classification of vortices in ^{3}He-B.

[14] T. Fujita, M. Nakahara, T. Ohmi, and T. Tsuneto, Prog. Theor. Phys. **60**, 671 (1978).

[15] V.K. Tkachenko, Zh. Éksp. Teor. Fiz. **49**, 1875 (1965) [Sov. Phys. JETP **22**, 1282 (1966)].

[16] E.B. Sonin, Rev. Mod. Phys. **59**, 87 (1987).

[17] E.V. Thuneberg, Phys. Rev. B **36**, 3583 (1987).

[18] E.B. Sonin and N.V. Fomin, Pis'ma Zh. Éksp. Teor. Fiz. **42**, 185 (1985) [JETP Lett. **42**, 229 (1985)].

[19] N.D. Mermin and T.-L. Ho, Phys. Rev. Lett. **36**, 594 (1976).

[20] A.J. Leggett, Ann. Phys. (N.Y.) **85**, 11 (1974).

[21] M.C. Cross, J. Low Temp. Phys. **21**, 525 (1975).

[22] J.W. Serene and D. Rainer, Phys. Rev. B **17**, 2901 (1978).

[23] E.V. Thuneberg and J.M. Karimäki, Physica B **194-196**, 777 (1994).

[24] M. Nakahara, T. Ohmi, T. Tsuneto, and T. Fujita, Prog. Theor. Phys. **62**, 874 (1979).

[25] A.L. Fetter, J.A. Sauls, and D.L. Stein, Phys. Rev. B **28**, 5061 (1983).

[26] A.L. Fetter, J. Low Temp. Phys. **58**, 545 (1985).

[27] X. Zotos and K. Maki, Phys. Rev. B **31**, 7120 (1985).

[28] K. Torizuka, J.P. Pekola, and A.J. Manninen, Physica B **178**, 244 (1992).

[29] G.E. Volovik and N.B. Kopnin, Pis'ma Zh. Éksp. Teor. Fiz. **25**, 26 (1977) [JETP Lett. **25**, 22 (1977)].

[30] T. Fujita and T. Ohmi, Czech. J. Phys. **46**, 1 (1996).

[31] G.E. Volovik and P.J. Hakonen, J. Low Temp. Phys. **42**, 503 (1981).

[32] H.K. Seppälä and G.E. Volovik, J. Low Temp. Phys. **51**, 279 (1983).

[33] X. Zotos and K. Maki, Phys. Rev. B **30**, 145 (1984).

[34] V.Z. Vulovic, D.L. Stein, and A.L. Fetter, Phys. Rev. B **29**, 6090 (1984).

[35] T. Ohmi, J. Low Temp. Phys. **56**, 183 (1984).

[36] H.K. Seppälä, P.J. Hakonen, M. Krusius, T. Ohmi, M.M. Salomaa, J.T. Simola, and G.E. Volovik, Phys. Rev. Lett. **52**, 1802 (1984).

[37] P.J. Hakonen, M. Krusius, and H.K. Seppälä, J. Low Temp. Phys. **60**, 187 (1985).

[38] K. Maki and X. Zotos, Phys. Rev. B **31**, 177 (1985).

[39] K. Maki and X. Zotos, Phys. Rev. B **31**, 3116 (1985).

[40] A.L. Fetter, J. Low Temp. Phys. **67**, 145 (1987).

[41] Ü. Parts, E.V. Thuneberg, G.E. Volovik, J.H. Koivuniemi, V.M.H. Ruutu, M. Heinilä, J.M. Karimäki, and M. Krusius, Phys. Rev. Lett. **72**, 3839 (1994).

[42] Ü. Parts, V.M.H. Ruutu, J.H. Koivuniemi, M. Krusius, E.V. Thuneberg, and G.E. Volovik, Physica B **210**, 311 (1995).

[43] J.W. Serene and D. Rainer, Phys. Rep. **101**, 221 (1983).

[44] P. Schiffer, M.T. O'Keefe, H. Fukuyama, and D.D. Osheroff, Phys. Rev. Lett. **69**, 3096 (1992).

[45] A.I. Ahonen, M. Krusius, and M.A. Paalanen, J. Low Temp. Phys. **25**, 421 (1976).

[46] K. Torizuka, J.P. Pekola, A.J. Manninen, and G.E. Volovik, Pis'ma Zh. Éksp. Teor. Fiz. **53**, 263 (1991) [JETP Lett. **53**, 276 (1991)].

[47] Ü. Parts, Y. Kondo, J.S. Korhonen, M. Krusius, and E.V. Thuneberg, Phys. Rev. Lett. **71**, 2951 (1993).